Elastic thermoelectric cells based on rubber, graphene and p-Bi_2Te_3 composites, fabricated by rubbing-in technology

KH. S. KARIMOV[a,b], M. SALEEM[c,*], N. FATIMA[d], R. ALI[a]
[a]*GIK Institute of Engineering Sciences and Technology, Topi, District Swabi, KPK, 23640, Pakistan*
[b]*Center for Innovative Development of Science and New Technologies of Academy of Sciences of Tajikistan, Dushanbe, 734025, Rudaki 33, Tajikistan*
[c]*Government Graduate College (B), Gulberg Lahore, 54000, Pakistan*
[d]*Solar Energy Research Institute, The National University of Malaysia, 43600 Bangi, Selangor, Malaysia*

The rubber, graphene and p-Bi_2Te_3 composite thermoelectric cells are fabricated and their properties are investigated. The cells were fabricated by deposition of the graphene nano powder and p-Bi_2Te_3 powder on the surface of porous rubber by use of rubbing-in technology. It was observed that Seebeck coefficient of the rubber and graphene composite decreased with increase of temperature, but in the case of the rubber, graphene and p-Bi_2Te_3 composite, it was increased. The output thermoelectric voltages of both composites increased with increase of the gradient of temperature. The thermoelectric voltage generated by the cell, fabricated from rubber and graphene composite was lower, at the same gradient of temperature, than that of the composite based on rubber, graphene and p-Bi_2Te_3. The rubbing-in technology can be used for the fabrication of the thermoelectric devices for demonstrative purpose. The obtained results may be used for the development of the flexible thermoelectric cells technology. The used technology for the cell's fabrication is simple and low cost.

(Received March 27, 2020; accepted June 11, 2021)

Keywords: Rubber, Graphene, p-Bi_2Te_3, Seebeck coefficient, Temperature gradient, Flexible substrate

1. Introduction

In the last years, thermoelectric cells and generators (TEGs) becoming more attractive for the researchers due to simplicity and cheapness in comparison with solar cells because of the absence of some kind of junction, as p-n, Schottky junctions or multiple junction structures [1,2]. At the same time, one of the most important point is the demonstration of a record high thermoelectric conversion efficiency of 8.5% that was recently shown in p-type MgAgSb-based compound which was operated in the temperature interval of (20 - 245) °C [3]. The efficiency can exceed 10% by increasing the hot side temperature to 295 °C which is comparable with solar cells efficiency. The sample was fabricated with silver contact pads using a one-step hot-press technique, eliminating a typically required sample metallization process. This significantly simplifies the fabrication of thermoelectric elements with low electrical and thermal contact resistances.

Efficiency (Z) of the thermoelectric cells is determined by the following relationship which was derived by Ioffe [4]:

$$Z = \frac{\sigma\alpha^2}{\kappa} \tag{1}$$

where σ is the electrical conductivity, κ is the thermal conductivity, and α is the Seebeck coefficient. Later, the dimensionless quantity, figure of merit (ZT) was introduced as well [5], with the average temperature:

$$\bar{T} = \frac{T_H + T_C}{2} \tag{2}$$

where T_H and T_C are temperatures of two contacts.

A greater ZT indicates a greater thermodynamic efficiency, subject to certain provisions, particularly that the two materials in the couple have similar efficiency. ZT is therefore a method for comparing the potential efficiency of devices using different materials. Values of 1 are considered good; values in the 3–4 range are essential for thermoelectrics to compete with mechanical devices in the efficiency. To date, the best reported ZT values are in around of 2 [6,7]. Much of the research in thermoelectric materials has focused on increasing of Seebeck coefficient and reducing κ by manipulating the nano-structure of the materials. Maximum energy efficiency is determined by:

$$\eta_{\max} = \frac{T_H - T_C}{T_H} \frac{\sqrt{1+ZT}-1}{\sqrt{1+ZT}+\frac{T_C}{T_H}} \tag{3}$$

Controlled oxidation level of reduced graphene oxides and its effect on thermoelectric properties were studied by Choi et al. [8]. In [9], higher thermoelectric performance of Bi_2Te_3 was obtained via defect engineering. The thermoelectric properties of the reduced graphene oxide /Bi_2Te_3 nanocomposites was investigated in [10] and it

was shown that Seebeck coefficient was negative, indicating n-type conduction. The Seebeck coefficient first increased and then decreased in the temperature interval from 25 °C to 300 °C. The thermal, electrical and thermoelectrical properties of graphene were reviewed in [11] and high thermoelectric power factor was observed in Graphene /hBN [12].

In recent past, we investigated elastic layered rubber-graphene composite fabricated by rubbing-in technology for the multifunctional sensors [13], semi-transparent photo-thermoelectric cells based on bismuth antimony telluride alloy [14]. Design, fabrication and investigation of semitransparent photo-thermoelectric cell with solar water collector for energy harvesting were presented in [15]. In [16], we studied the semitransparent thermo-electric cells, based on bismuth telluride and its composites with CNTs and graphene. In continuation of our efforts for the investigation of the thermoelectric properties of the graphene and telluride containing composites, we are presenting in this paper the properties of the elastic thermoelectric cells based on rubber, graphene and p-Bi_2Te_3 composites, fabricated by rubbing-in technology.

2. Experimental

In Fig. 1, the X-ray diffraction results are presented. Each diffraction data (rubber, graphene and bismuth antimony telluride) was obtained three times to check the repeatability.

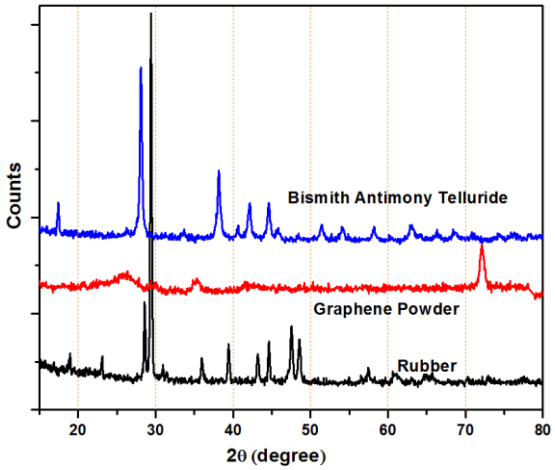

Fig. 1. XRD patterns of original rubber, graphene powder and bismuth antimony telluride (color online)

The XRD pattern of rubber shows notable high intensity Bragg's diffraction peaks at 2θ of 23.1°, 29.4° and 36°, respectively. These peaks and other peaks present in the rubber XRD diffractogram are characteristics of polyvinyl chloride which correspond to high amount of structural arrangement (order) in its polymeric chains [17]. The peaks of graphite were observed around 26.60° corresponding to the graphitic structure (002) and was consistent with standard XRD data (ICSD code: 0250284). The major peaks of bismuth antimony telluride (p-type) was observed at 2θ of 28.11°, which is consistent with standard XRD data (PDF 049-1713) [18].

For the fabrication of the samples, the rubber substrate, graphene powder and p-Bi_2Te_3 powder were used. In Fig. 2, the fabrication of graphene and p-Bi_2Te_3 composites films by rubbing-in technology is shown. The rubber substrate sizes were 30 mm × 5 mm × 5 mm. In this process, the rubber substrate was covered uniformly by powder of graphene and by densifier the powder, in order to fabricate rubber-graphene composite. The thermoelectric measurements of the fabricated, rubber-graphene composite cell were recorded.

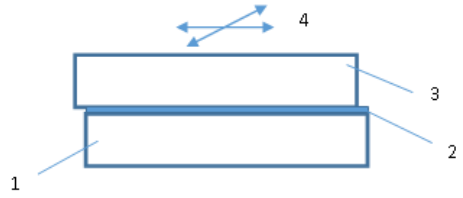

Fig. 2. Fabrication of graphene and p-Bi_2Te_3 composites films by rubbing-in technology: rubber substrate (1), graphene and p-Bi_2Te_3 films (2), cylindrical rubber densifier (3) and motion of densifier in horizontal plane (4) (color online)

After the thermoelectric experiments on rubber substrates coated by graphene films, on the same graphene film, p-Bi_2Te_3 film was deposited by rubbing-in technology as well. It was done in order to identify the total effect of the graphene and p-Bi_2Te_3 film on the thermoelectric properties of the samples. The thickness of each of these films was equal to 10-12 μm. In this process, the pressure of the densifier to graphene powder was in the range of (40-50) gf/cm^2. Velocity of the densifier's motion along the two horizontal axes, was in the range of (0.5-1.0) cm/sec. Fig. 3 shows the elastic thermoelectric cell based on rubber, graphene and p-Bi_2Te_3 composites fabricated by rubbing-in technology. The elastic thermoelectric cells based on rubber and p-Bi_2Te_3 composites only without of graphene layer was also fabricated by rubbing-in technology. Due to high resistance of these cells, it was not possible to measure the thermoelectric voltage developed in these samples.

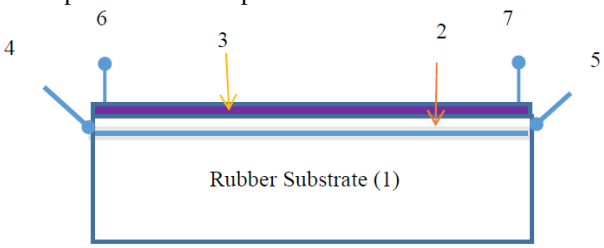

Fig. 3. Elastic Thermoelectric Cells Based on Rubber, Graphene and p-Bi_2Te_3 composites fabricated by rubbing-in technology: rubber substrate (1), graphene film (2), p-Bi_2Te_3 film (3), thermocouples (4 and 5), terminals (6 and 7) (color online)

Fig. 3 shows the schematic diagram of the elastic thermoelectric cells based on rubber, graphene and p-Bi_2Te_3 composites, fabricated by rubbing-in technology:

rubber substrate (1), graphene film (2), p-Bi_2Te_3 film (3), thermocouples (4 and 5), and terminals (6 and 7).

3. Results and discussions

Fig. 4 shows relationships between thermoelectric voltage (V) developed by the rubber-graphene composite and rubber-graphene- p-Bi_2Te_3 composite samples and gradient of temperature (ΔT). It is seen that both curves are quasi-sub linear: the voltages increased with increase of temperature gradient. The thermoelectric voltage developed in the rubber-graphene- p-Bi_2Te_3 composite samples is higher than that of the voltage in the case of rubber-graphene composite sample. It is obviously due to presence of p-Bi_2Te_3 in the composite.

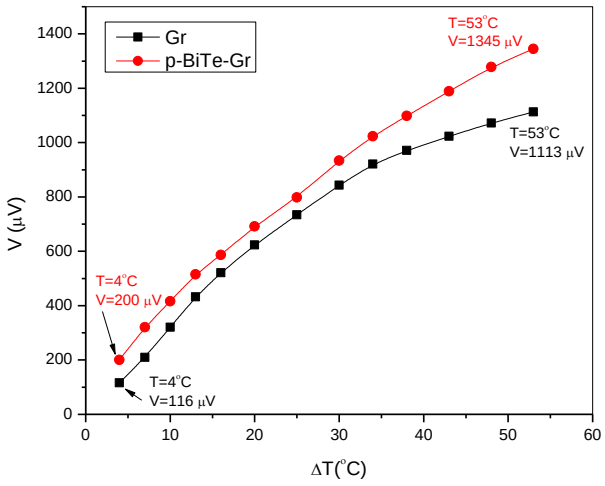

Fig. 4. Relationships between voltages and gradient of temperature in rubber-graphene- composite and rubber-graphene- p-Bi_2Te_3 composite samples (color online)

Fig. 5 shows relationships between Seebeck coefficient and temperature received in the rubber-graphene composite and rubber-graphene- p-Bi_2Te_3 composite samples. Fig. 5 shows that Seebeck coefficients (Δα) and temperature relationships of the rubber-graphene composite and rubber-graphene-p-Bi_2Te_3 composite. As the temperature increased, Seebeck coefficient of the rubber-graphene composite decreased unlike to the case of the rubber-graphene- p-Bi_2Te_3 composite.

The thermoelectric properties of Bi_2Te_3 and n-type Bi_2Te_3, co-doped with x at % CuI and ½x at % Pb (x = 0, 0.01, 0.03, 0.05, 0.07, and 0.10) were investigated by Han et al. [19]. In these results, it was found that, in the temperature range from 300 K to 523 K, Seebeck coefficient of undoped Bi_2Te_3 decreased with increase of temperature from -270 μV/K to -25 μV/K. In heavily doped Bi_2Te_3 (10% CuI-Pb), the Seebeck coefficient slightly increased from -80 μV/K to -110 μV/K.

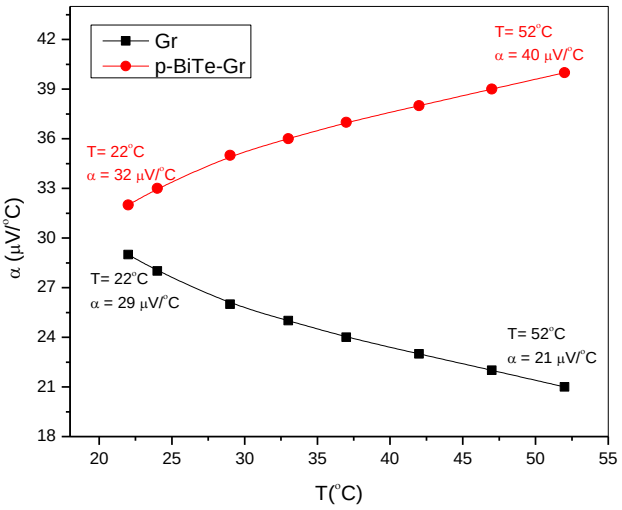

Fig. 5. Relationship between Seebeck coefficient (α) and temperature (T), received in the rubber-graphene composite and rubber-graphene-p-Bi_2Te_3 composite samples (color online)

Experimental and theoretical results on the thermoelectric properties of graphene and its nanostructures were reviewed by Dollfus et al. [20]. It is stated that Seeback effect in graphene is lower as graphene is gapless and contribution of electrons and holes are opposite and ZT is very limited. Nevertheless, it was discussed also the thermoelectric properties of the hybrid graphene structures, as graphene, layered carbon allotropes as graphynes, graphdiynes, and graphene/ hexagonal boron nitride heterostructures. These structures offer new opportunities for further development 2D semiconductors with finite bandgap, i.e. dichalcogenides and phosphorene, which can be used in thermoelectric technology.

The rubber-graphene-p-Bi_2Te_3 thermoelectric cell structure, investigated by us, can be represented as graphene, p-Bi_2Te_3 and interface between of these two layers structure which may be replaced by the following equivalent circuit, where I_1, I_2 and I_3 are corresponding current sources (Fig. 6). Probably one of the most important and interesting layers is interface between graphene and p-Bi_2Te_3, where in principle, due to collective oscillations of electrons [20-23], the waveguide may be formed which can crucially increase thermoelectric effect.

The Seebeck coefficient for metals and degenerate semiconductors can be described by the following Equation [24]:

$$S = m^* T \frac{8\pi^2 K_B^{\,2}}{3eh^2}\left(\frac{\pi}{3n}\right)^{\frac{2}{3}} \qquad (4)$$

where m^* is the effective mass of the carrier, h is the Planck constant, and K_B is the Boltzmann constant. The carrier scattering and the carrier concentration influence crucially to the Seebeck coefficient of the composites. The Seebeck coefficient dependences on temperature is shown in Fig. 6. For rubber-graphene- p-Bi_2Te_3 composite in the

first approximations, can be explained accordingly by increase of the temperature mostly and effects related to it. In the case of rubber-graphene composite for the explanation of the decrease of the Seebeck coefficient with increase of the temperature, probably it is needed additional data concerning dependence of the effective mass on temperature.

At present, the elastic, stretchable or deformable electronics is developing in particular described in [25-27], that will allow to fabricate different devices for different applications, including conformable for human body, electronic devices for particular applications, as presented in this paper, for measurement, for example, of temperature gradient that can be potentially realized by use of elastic thermoelectric cells based on rubber, graphene and p-Bi_2Te_3 composites.

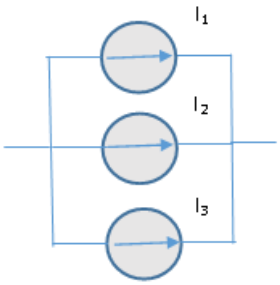

Fig. 6. Equivalent electric circuit of the rubber-graphene-p-Bi_2Te_3 thermoelectric generator, shown as currents I_1, I_2 and I_3 representing graphene layer, p-Bi_2Te_3 layer and interface between graphene-p-Bi_2Te_3 (color online)

Table 1. Comparison of the obtained results with existing research related to thermoelectric effect in the investigated materials

Sr. #	**Presented (in the paper) results**	**Obtained results in literature**
1.	Relationships between thermoelectric voltage and gradient of temperature of rubber graphene composite and rubber-graphene- p-Bi_2Te_3 composite samples (Fig. 4).	Improving thermoelectric properties of p-type Bi_2Te_3-based alloys by spark plasma sintering [28].
2.	Relationships between Seebeck coefficient and temperature received in the rubber-graphene composite and rubber-graphene-p-Bi_2Te_3 composite samples (Fig. 5).	P-type bismuth telluride-based composite thermoelectric materials produced by mechanical alloying and hot extrusion [29].
3.		Thermoelectric properties of p-type $(Bi_2Te_3)_{0.2}(Sb_2Te_3)_{0.8}$ thermoelectric material doped with PbTe [30].
4.		Shifting up the optimum figure of merit of p-type bismuth telluride–based thermoelectric materials for power generation by suppressing intrinsic conduction [31].
5		Bi_2Te_3–based applied thermoelectric materials: research advances and new challenges [32].
6.		Review of development status of Bi_2Te_3–based semiconductor thermoelectric power generation [33].

Comparison of the obtained results with published data given in Table 1 concerning p-type Bi_2Te_3 based thermoelectric materials show that our findings, presented in this paper, bring new additional information concerning**,** in particular**,** rubber graphene composite and rubber-graphene- p-Bi_2Te_3 composite based thermoelectric cells.

4. Conclusion

In this paper, the properties of the elastic thermoelectric cells based on rubber, graphene and p-Bi_2Te_3 composites, fabricated by rubbing-in technology were investigated. It was observed that the thermoelectric properties of the rubber-graphene composite can be improved by adding Bi_2Te_3 in the composite layer. At present, the elastic, stretchable or deformable electronics is developing, that will allow to fabricate different devices for different applications, including conformable for human body, electronic devices for particular applications, as presented in this paper, for measurement, for example, of temperature gradient that can be potentially realized by use of elastic thermoelectric cells based on rubber, graphene and p-Bi_2Te_3 composites. It should be mentioned that the developed technology (rubbing-in) that was used for the fabrication of the thermoelectric cells, which were investigated in this paper, is simple, low cost, easier and can be realized in the laboratories conditions.

Acknowledgements

The authors acknowledge with thanks the authority of GIK Institute of Pakistan for technical and financial support.

References

[1] Kh. S. Karimov, Dr. J. N. Govil (Ed.) Energy Science and Technology, Studium Press LLC, U.S.A., 302 (2015).
[2] Kh. S. Karimov, M. Abid, K. Y. Cheong, M. M. Bashir, Thermoelectric properties of organic and inorganic materials and cells, Two-dimensional nanostructures for energy-related applications, K. Y. Cheong (Ed.), Taylor & Francis Group, Boca Raton, Landon, New York, 48 (2017).
[3] D. Kraemer, J. Sui, K. McEnaney, H. Zhao, Q. Jie, Z. F. Ren, G. Chen, Energy Environ. Sci. **8**, 1299 (2015).
[4] A. F. Ioffe, Dokl. Acad. Nauk. USSR **87**, 369 (1952).
[5] A. Bulusu, D. G. Walker, Superlattices Microstruct. **44**, 1 (2008).
[6] K. F. Hsu, S. Loo, F. Guo, W. Chen, J. S. Dyck, C. Uher, T. Hogan, E. Polychroniadis, M. G. Kanatzidis, Science **303**, 818 (2004).
[7] K. Biswas, J. He, I. D. Blum, C. I. Wu, T. P. Hogan, D. N. Seidman, V. P. Dravid, M. G. Kanatzidis, Nature **489**, 414 (2012).
[8] J. Choi, N. D. K. Tu, S. S. Lee, H. Lee, J. S. Kim, H. Kim, Macromolecular Research **22**, 1104 (2014).
[9] Y. Liu, M. Zhou, J. He, Scripta Materialia **111**, 39 (2016).
[10] Y. Du, J. Li, J. Xu, P. Eklund, Energies **12**, 2430 (2019).
[11] J. Wang, X. Mu, M. Sun, Nanomaterials **9**, 218 (2019).
[12] J. Duan, X. Wang, X. Lai, G. Li, K. Watanabe, T. Taniguchi, M. Zebarjadi, E. Y. Andrei, High thermoelectric power factor in Graphene /hBN devices, Proceedings of the National Academy of Sciences. 113. 10.1073/pnas.1615913113 (July 2016).
[13] Kh. S. Karimov, Z. Ahmad, M. I. Khan, K. J. Siddiqui, T. A. Qasuria, S. Z. Abbas, M. Usman, A. Rehman, Heliyon **5**, eo1187 (2019).
[14] Kh. S. Karimov, N. Fatima, T. A. Qasuria, K. J. Siddiqui, M. M. Bashir, Y. S. Alharthi, H. F. Alharbi, N. H. Alharthi, N. Amin, Md. Akhtaruzzaman, J. Alloys Comp. **816**, 152593 (2020).
[15] M. M. Bashir, Kh. S. Karimov, J-U Nabi, N. Fatima, R. Ali, Int. J. Electrochem. Sci. **14**, 8544 (2019).
[16] Kh. S. Karimov, J-U. Nabi, H. Meng, Z. Ahmad, M. Riaz, M. M. Bashir, M. I. Khan, R. Ali, A. Khan, F. Touati, J. Optoelectron. Adv. M. **21**(5-6), 333 (2019).
[17] I. P. Ejidike, C. W. Dikio, D. Wankasi, E. D. Dikio, F. M. Mtunzi, Int. J. Environ. Studies **75**, 932 (2018).
[18] J. J. Ritter, P. Maruthamuthu, Inorg. Chem. **36**, 260 (1997).
[19] M. K. Han, Y. Jin, D. H. Lee, S. J. Kim, Materials **10**, 1235 (2017).
[20] P. Dollfus, V. H. Nguyen, J. S. Martin, J. Phy. Cond. Matter **27**, 133204 (2015).
[21] S. A. Mikhailov, K. Ziegler, Phys. Rev. Lett. **99**, 016803 (2007).
[22] M. Jablan, H. Buljan, M. Soljačić, Phys. Rev. B **80**, 245435 (2009).
[23] G. W. Hanson, J. Appl. Phys. **103**, 064302 (2008).
[24] G. J. Snyder, E. S. Toberer, Nat. Mater. **7**, 105 (2008).
[25] W. Yuan, X. Wu, W. Gu, J. Lin, Z. Cui, J. Semicond. **39**, 015002 (2018).
[26] B. Liang, Z. Zhang, W. Chen, D. Lu, L. Yang, R. Yang, H. Zhu, Z. Tang, X. Gui, Nano-Micro Letters **11**, 92 (2019).
[27] J. Xin, C. Xu-Dong, W. Wen-Yu, Z. Zheng-Tao, L. Tong, J. Materials Engin. **46**, 13 (2018).
[28] D. Li, R. Sun, X. Qin, Progress in Natural Sci.: Mater. Int. **21**, 336 (2011).
[29] M. K. Keshavarz, D. Vasilevskiy, R. A. Masut, S. Turenne, J. Elec. Materi. **42**, 1429 (2013).
[30] D. Kusano, Y. Hori, J. Japan Inst. Metals **66**, 1063 (2002).
[31] L. P. Hu, T. J. Zhu, Y. G. Wang, H. H. Xie, Z. J. Xu, X. B. Zhao, NPG Asia Mater. **6**, e88 (2014).
[32] J. Pei, B. Cai, H. L. Zhuang, J. F. Li, Natl. Sci. Rev. **7**, 1856 (2020).
[33] Y. Chen, X. Hou, C. Ma, Y. Dou, W. Wu, Adv. Mater. Sci. Eng. **2018,** 1210562, (2018).

*Corresponding author: msaleem108@hotmail.com; muh.saleem@gmail.com